Using Support Vector Machines with Tract-Based Spatial Statistics for Automated Classification of Tourette Syndrome Children

Hongwei Wen[1,2a], Yue Liu[3,4a], Jieqiong Wang[1], Jishui Zhang[3,4], Yun Peng[3,4*], Huiguang He[1,2*]
[1] State Key Laboratory of Management and Control for Complex Systems, Institute of Automation, Chinese Academy of Sciences, Beijing, China
[2] Research Center for Brain-inspired Intelligence, Institute of Automation, Chinese Academy of Sciences, Beijing, China
[3] Department of Radiology, Beijing Children's Hospital, Capital Medical University, Beijing, China
[4] Beijing key Lab of Magnetic Imaging Device and Technique, Beijing Children's Hospital, Capital Medical University, Beijing, China

ABSTRACT

Tourette syndrome (TS) is a developmental neuropsychiatric disorder with the cardinal symptoms of motor and vocal tics which emerges in early childhood and fluctuates in severity in later years. To date, the neural basis of TS is not fully understood yet and TS has a long-term prognosis that is difficult to accurately estimate. Few studies have looked at the potential of using diffusion tensor imaging (DTI) in conjunction with machine learning algorithms in order to automate the classification of healthy children and TS children. Here we apply Tract-Based Spatial Statistics (TBSS) method to 44 TS children and 48 age and gender matched healthy children in order to extract the diffusion values from each voxel in the white matter (WM) skeleton, and a feature selection algorithm (ReliefF) was used to select the most salient voxels for subsequent classification with support vector machine (SVM). We use a nested cross validation to yield an unbiased assessment of the classification method and prevent overestimation. The accuracy (88.04%), sensitivity (88.64%) and specificity (87.50%) were achieved in our method as peak performance of the SVM classifier was achieved using the axial diffusion (AD) metric, demonstrating the potential of a joint TBSS and SVM pipeline for fast, objective classification of healthy and TS children. These results support that our methods may be useful for the early identification of subjects with TS, and hold promise for predicting prognosis and treatment outcome for individuals with TS.

Keywords: Tourette syndrome, DTI, Tract-Based Spatial Statistics, ReliefF, SVM

1. INTRODUCTION

Tourette syndrome (TS) is a neurological disorder that emerges in early childhood (3-8 years) and which is characterized by involuntary and repetitive motor and vocal tics. For most patients, the worst tic severity falls between 7-15 years of age. TS is frequently concomitant with obsessive-compulsive disorder (OCD), attention-deficit hyperactivity disorder (ADHD), and other social and behavioral disturbances. To date, the neural basis of TS remains largely unknown. However, increasing evidence from experimental, electrophysiological and imaging studies points to abnormalities within the fronto-striato-thalamic pathways [1, 2]. While tics constitute the major diagnostic symptom, TS is quite heterogeneous and has a long-term prognosis that is difficult to accurately estimate. Moreover, the current practice in the diagnosis of TS is mainly according to the levels of symptoms listed in Diagnostic and Statistical Manual of Mental Disorders (DSM) criteria [3], and the diagnosis is usually conducted by the parents, which is unfortunately subjective. Thus, further studies on objective diagnosis of TS are of great significance.

Diffusion Tensor Imaging (DTI) is becoming widely used for its high sensitivity in detecting micro-structural alterations and reconstructing white matter (WM) tracts via estimating main fiber orientation. Tract-Based Spatial Statistics (TBSS)

[a] These authors contributed equally to this work. [*] Correspondence to:
Huiguang He: Research Center for Brain-inspired Intelligence, Institute of Automation, Chinese Academy of Sciences, Beijing, 100190, China. E-mail: huiguang.he@ia.ac.cn
Yun Peng: Department of Radiology, Beijing Children's Hospital, Capital Medical University. No.56 Nanlishi Road, West District, Beijing, 100045, China. E-mail: ppengyun@yahoo.com

Medical Imaging 2016: Computer-Aided Diagnosis, edited by Georgia D. Tourassi, Samuel G. Armato III,
Proc. of SPIE Vol. 9785, 97852Q · © 2016 SPIE · CCC code: 1605-7422/16/$18 · doi: 10.1117/12.2216647

analysis of DTI data was recently developed as an automatic, hypothesis-free and precise method for the assessment of integrity of the WM [4]. Some previous studies have used TBSS to indicate that significant axial diffusivity (AD) and mean diffusivity (MD) increases were found in anterior thalamic radiation, right cingulum bundle projecting to the cingulate gurus and forceps minor in early TS children [5]. To date, machine learning techniques have been applied to a range of MRI modalities in an effort to automate the diagnosis of disease [6, 7]. However, few studies have looked at the potential of combining them to earliest phase diagnosis of TS which may be a key to discovering etiology, prevention or treatment. In our study, we aimed to take a first step toward this goal and make diagnostic predictions about individuals using DTI. We applied support vector machine (SVM) classification with TBSS to assess the efficacy of each DTI metric for classification and the locations of the voxels that were most useful for discriminating between groups. SVM classification takes a multivariate approach that can be sensitive to detecting group differences in patterns of data that may go unseen by traditional univariate analyses.

2. MATERIALS AND METHODS

2.1 Subjects

44 TS patients were recruited from outpatient clinics in Beijing Children's Hospital from July 2012 to May 2015 (age: 8.98±3.114 years, range: 3–16 years; 11 female). All the patients met DSM-IV-TR (Diagnostic and Statistical Manual of Mental Disorders, 4th Edition, text revision) criteria for TS. We also included 48 age and gender matched health controls in our study (age: 11.00±3.495 years; range: 3–17 years; 17 female). We used a clinical interview and the Children's Yale-Brown Obsessive Compulsive Scale (CY-BOCS) to diagnose OCD and used the German short version of Wender Utah rating scale (WURS-k, translated to Chinese) to diagnose ADHD. Patients fulfilling OCD criteria or other co-morbidities were excluded from the study. Tic severity for all patients was rated using the Yale Global Tic Severity Scale (YGTSS) and ranged from 10 to 79 ([mean±SD]: 46.50±18.037). The duration of TS ranged from 3 month to 5 years ([mean±SD]: 1.81±1.423 years). For those who had course less than 1 year, TS diagnosis was made by follow-up call. After the study was approved by Beijing Children's Hospital review board, written informed consent was obtained from all the parents/guardians according to the Declaration of Helsinki.

2.2 Data acquisition

Magnetic resonance imaging was acquired using a 3.0T MR scanner (Gyroscan Interna Nova, Philips, Netherland). Head positioning was standardized using canthomeatal landmarks. The head was stabilized with foam pads to minimize head movements. Patients were instructed to suppress tics and minimize head movements during scanning as much as possible. Axial three-dimensional diffusion tensor imaging (DTI) was acquired from all the subjects. DTI was performed using the following protocol: spin-echo diffusion-weighted echo-planar imaging sequence, 2mm slice thickness, no inter-slice gap, repetition time = 4300ms, echo time = 95ms, field of view (FOV) =255×255mm, reconstructed image matrix = 336×336. Diffusion MRI images were obtained from 30 non-collinear directions with a b value of 1000 s/mm^2.

2.3 Data preprocessing

Following image acquisition, we used the FMRIB's Diffusion Toolbox (FDT2.0) within FSL v4.1 (http://www.fmrib.ox.ac.uk/fsl) for DTI processing. For each participant, 30 DTI volumes with 1000s/mm^2 b-value were first affinely registered to the b0 volume for correction of eddy current distortion and simple head motion. Non-brain voxels were removed using Brain Extraction Tool (BET) of FSL; a fractional intensity threshold of 0.25 was selected, resulting in a brain-extracted 4D image and a binary brain mask for each subject. We then used the eddy-corrected 4D data and corresponding brain mask to fit the diffusion tensor model at each voxel by using the FDT. Eigenvalues of diffusion tensor matrix (λ_1, λ_2, λ_3) were obtained and maps of axial diffusivity (AD=λ_1), mean diffusivity (MD=(λ_1+λ_2+λ_3)/3), and fractional anisotropy (FA) were generated. Radial diffusivity (perpendicular eigenvalue, λ_{23}= (λ_2+λ_3)/2) was calculated by averaging λ_2 and λ_3 maps.

2.4 Tract-Based Spatial Statistics

The Most-Representative-Subject TBSS (RS-TBSS) procedure[8] was then applied to the data which is recommended if the subjects are all young children. The FA images from each participant were co-registered to every other one using a nonlinear registration (FNIRT) provided by FSL, identify the "most representative" one, and use this as the target image. This target image is then affine-aligned into MNI152 standard space, and every image is transformed into 1×1×1 mm

MNI152 space by combining the nonlinear transform to the target FA image with the affine transform from that target to MNI152 space. The resulting standard-space FA images of each participant were averaged to create a mean FA image, and then a skeleton image of WM tracts was created suppressing all non-maximum FA values in each voxel's local-perpendicular direction and subsequently comparing all remaining non-zero voxels with their nearest neighbors, thus searching for the center of fiber bundles. A threshold of 0.2 was selected to define the border distinguishing white from gray matter. Then, for each participant, we projected the local maximal FA intensity along the perpendicular direction of the WM tract to the mean FA skeleton to carry out the voxel wise statistics across subjects. The same projection method was applied to MD, AD, and RD images. For voxel-wise group comparisons between patients and normal control on the skeleton image, we used FSL's randomise tool. Essentially, randomise uses a permutation-based statistical inference that does not rely on a Gaussian distribution. Random Monte Carlo simulated samples of 10,000 permutations were used as null distribution. $P<0.05$ were identified as significant and corrected for multiple comparisons with threshold-free cluster enhancement (TFCE) method[9] to avoid definition of an initial cluster-forming threshold or carrying out a large amount of data smoothing (Figure 1 shows the pipeline). The *ICBM-DTI-81 white-matter labels* atlas, *JHU White-Matter Tractography* atlas and *Talairach Daemon Labels* atlas provided by FSL were used to identify the abnormal white matter tracts. Similarly, we also analyze MD, RD and AD TBSS results.

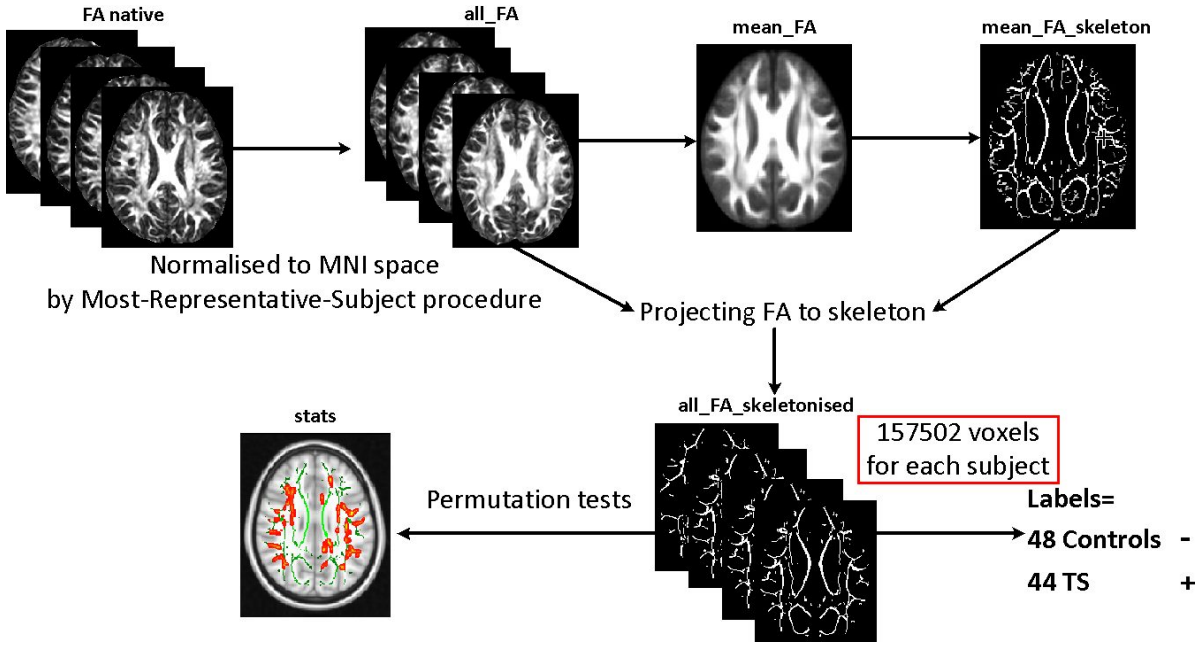

Figure 1. **Flow-chart of the RS-TBSS procedure.** A WM skeleton is created in TBSS processing which is common to all subjects. Diffusion values are then extracted from every voxel in the WM skeleton. Data is then labelled as either Control or TS.

2.5 Feature selection

Following TBSS analysis, a mask was created based on the WM skeleton that is common to all subjects and the skeletonised FA, AD, RD and MD images were analysed in Matlab. There were 157502 voxels in the WM skeleton and diffusion values for each DTI metric were extracted from each voxel in the WM skeleton. Classification between groups was undertaken using each DTI metric separately in order to determine the most efficient metric for classification.

Feature selection was to reduce the number of voxels to those that are most relevant for classification. This step eliminates non-discriminative voxels which would reduce classification accuracy. The feature selection algorithm ''ReliefF''[10] was used to extract the most salient voxels. The basic idea of ReliefF is to draw instances at random, compute their nearest neighbors, and adjust a feature weighting vector to give more weight to features that discriminate the instance from neighbors of different classes. Given a set of training sample data $X=\{x_1,x_2,\ldots\ldots x_n\}$, $x_i=\{x_{i1},x_{i2},\ldots\ldots x_{iN}\}^T$, x_{iN} is the Nth feature value of the ith sample, λ is a $N\times1$ matrix, representing the weight of each feature. ReliefF searches for R nearest neighbors from the same class called nearest hits h_j, $j=1,2,\ldots\ldots R$, and also R

nearest neighbors from each of the different classes, called nearest misses m_{ij}, j=1,2,……R, l≠class(x_i). Assuming that diff_hit is a N×1 matrix, representing the difference between hj and xi on feature.

$$\text{diff\_hit} = \sum_{j=1}^{R} \frac{|x_i - h_j|}{\max(X) - \min(X)} \tag{1}$$

Assuming that diff_miss is a N×1 matrix, representing the difference between m_{lj} and x_i on feature.

$$\text{diff\_miss} = \sum_{l \neq \text{class}(x_i)} \frac{P(l)}{1 - P(\text{class}(x_i))} \sum_{j=1}^{R} \frac{|x_i - m_{lj}|}{\max(X) - \min(X)} \tag{2}$$

where P(l) is the probability of class l, ReliefF then updates the weight λ based on the formulation.

$$\lambda = \lambda - \frac{\text{diff\_hit}}{R} + \frac{\text{diff\_miss}}{R} \tag{3}$$

For each classification group and also for each DTI metric, nine reduced feature sets were created, containing 100 voxels, 250 voxels, 500 voxels, 750 voxels, 1000 voxels, 2000 voxels, 3000 voxels, 4000 voxels and 5000 voxels respectively. The choice of identifying these 9 feature sets is based on previous studies that have shown that this is an optimum range of data reduction for successful classification [11, 12]. However, compared to their method, our method employs feature selection on the training samples rather than the entire samples.

2.6 Classification

After reducing the features into feature sets of differing sizes, classification was then performed using the SVM algorithm sequential minimal optimization (SMO) with a radial basis function (RBF) kernel. We use a nested 10-fold cross-validation strategy to evaluate the classification performance. For outer CV, the data is randomly divided into 10 parts in which each class is represented in approximately the same proportions as in the full sample. Each fold is held out in turn and the learning scheme trained on the remaining nine-tenths and the error rate is then calculated on the tenth fold. Following 10 training procedures, the 10 error rates are averaged to yield an overall error estimate and we consider it as the estimation of generalization [13]. We performed another ten-fold cross-validation on the training samples which is called inner CV. To estimate suitable values for C and σ we used a grid search in the range of $C=2^{-4}, 2^{-1}, ..., 2^{4}$ and $\sigma = 2^{-8}, 2^{-7}, ..., 2^{2}$. C is penalized coefficient that adjusts the importance of the separation error in the creation of the separation surface, and σ represents the width of the radial basis function. Classification accuracy was evaluated via 10-fold cross validation to ensure performance generalization. The workflow of the reduction of the voxels using ReliefF and the application of the SVM is shown in Figure 2.

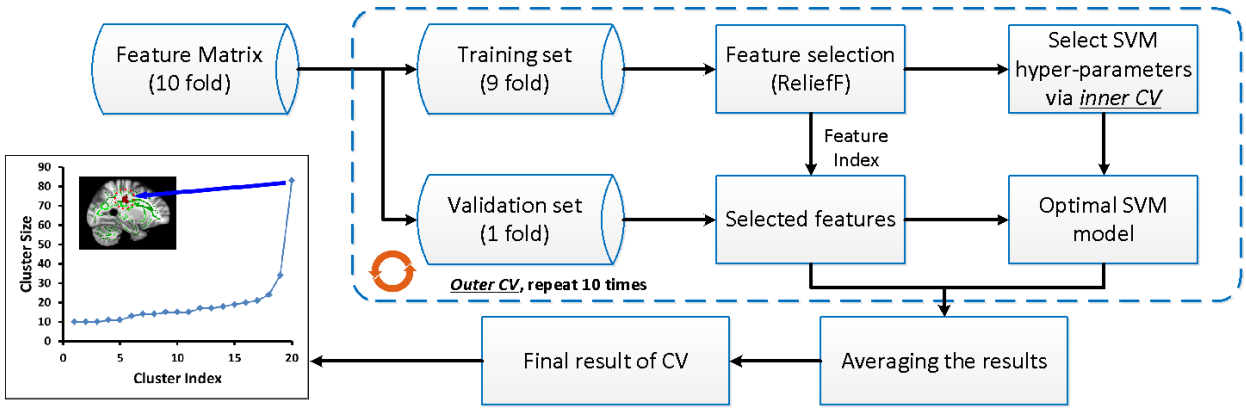

Figure 2. **The flow chart of the nested CV classification method using each diffusion metric.** Following feature extraction from the WM skeleton, the feature set is reduced using a feature selection algorithm, ReliefF. This algorithm selects the most salient voxels for group classification. These voxels are then used for training a SVM classifier with a 10-fold cross validation. The bottom left figure shows the readout of top 2000 voxels selected from the full AD feature set. The y-axis represents the size of particular clusters and the location of the largest cluster is shown circled in red in the anatomical images.

For the analysis of results, accuracy, sensitivity, specificity and the area under the curve for the receiver operated characteristic curve (AUC ROC) are shown. Accuracy is defined as (TP+TN)/(TP+TN+FN+FP) where TP = True Positive, TN =True Negative, FP = False Positive and FN = False Negative. Sensitivity is defined as TP/(TP+FN) and Specificity is defined as TN/(FP+TN).

3. RESULTS

3.1 Quantification of microstructural changes with TBSS

Compared with healthy control children, TS children showed significantly ($p<0.05$, corrected for multiple comparisons) reduced FA, increased RD and MD in multiple white matter skeleton clusters. We did not find any significant FA increase, RD and MD decreases compared with healthy children. Skeleton clusters showing no significantly changed AD at $p<0.05$ (corrected for multiple comparisons)(Figure 3). However, there was a trend towards higher AD values in TS children relative to healthy control children ($p<0.05$, not corrected for multiple comparisons).

3.2 SVM Classification of Control and TS

For the classification of control and TS children, the accuracy (88.04%), sensitivity (88.64%) and specificity (87.50%) were achieved in our method as peak performance of the SVM classifier was achieved using the AD metric with 2000 voxels feature set. For the FA metric, classification performance was slightly lower, with accuracy in the range of 68–86%. For RD and MD metrics, classification performance had the accuracy in the range of 65–85% (Figure 4 shows all the measures). As peak performance was achieved the feature set of 2000 voxels, the ROC curve is shown for this feature set for all 4 DTI metrics (Figure 5).

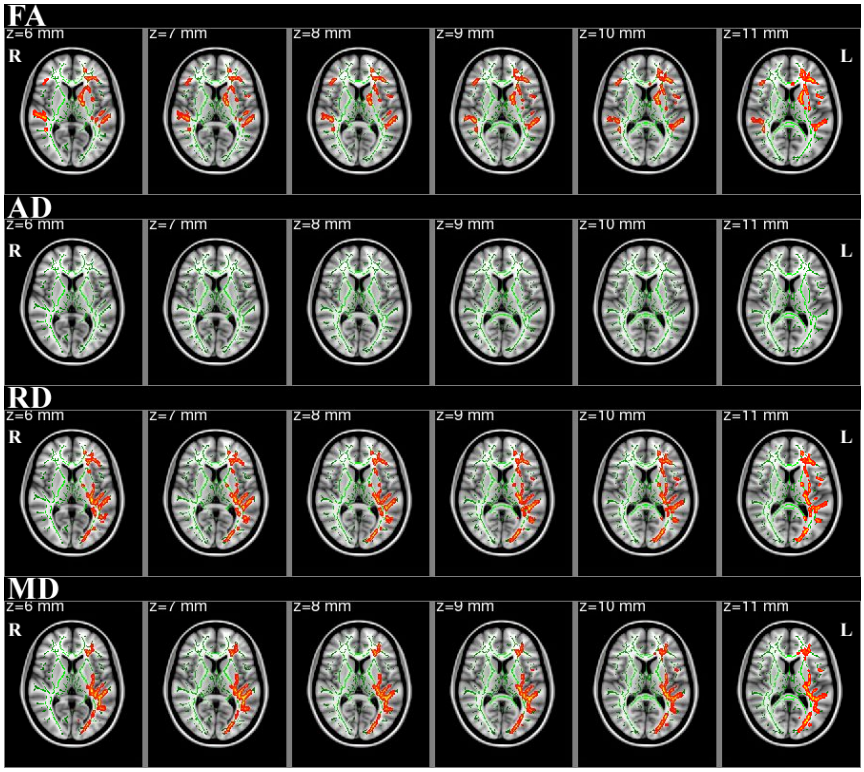

Figure 3. **The identified significantly changed ($p<0.05$, family-wise error corrected for multiple comparisons) FA, AD, RD and MD skeleton clusters were filled (using tbss_fill script implemented in FSL) to make the presentation easy.** The background image is the standard MNI_T1_1mm template and the FA skeleton (green). Red-Yellow voxels represent regions in which FA was decreased significantly; RD and MD were increased significantly in TS children relative to healthy controls. Skeleton clusters showing no significant AD change. Axial slices from Z = 6 to 11 in MNI coordinate are shown.

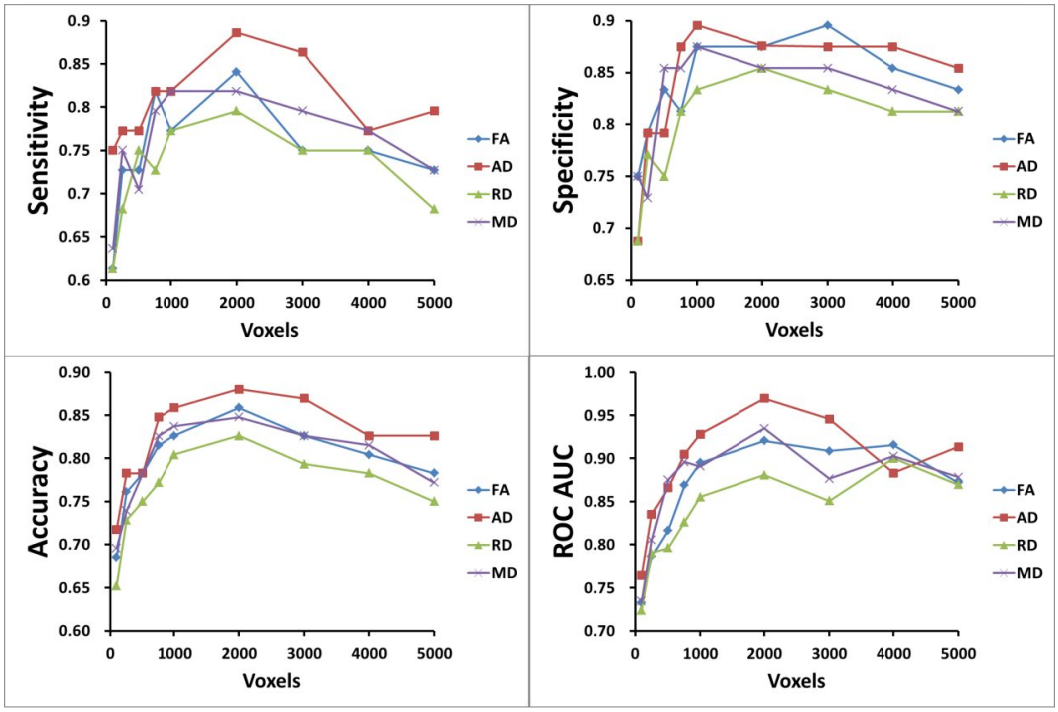

Figure 4. **Sensitivity, specificity, accuracy and the area under the curve for a receiver operating characteristic curve (ROC AUC) for control and TS children classification.** Results are shown for the 9 feature sets – 100 voxels, 250 voxels, 500 voxels, 750 voxels, 1000 voxels, 2000 voxels, 3000 voxels, 4000 voxels and 5000 voxels. The voxels comprising these reduced feature sets were selected by the ReliefF algorithm.

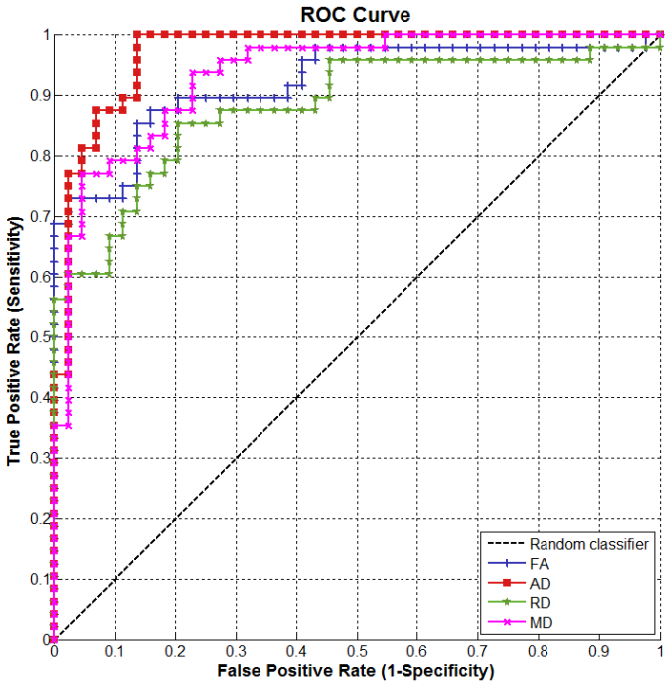

Figure 5. **Comparison of ROC curve under the peak performance of the SVM classifier which occurs with feature set of 2000 voxels.** True positives refer to TS children that are correctly classified as TS, and false positives refer to healthy children that are incorrectly labelled as TS. The best classification performance was achieved using the AD metric.

3.3 Regions Most influential for Classification

Following classification, we subsequently created images depicting the location of some of clusters of voxels selected the ReliefF algorithm. For the control and TS children classification, we chose the AD feature set with the top 2000 voxels that produced the highest accuracy, sensitivity and specificity. Using *cluster* command provided by FSL, we present the largest 5 clusters (size≥20) of voxels selected by ReliefF. The coordinates of the local maxima and cluster size are listed in Table 1.

Table 1. Skeleton clusters selected by the ReliefF algorithm as the most salient for group classification.

Skeleton clusters	Cluster	MNI Coordinates(mm)		
	size	x	y	z
Left corticospinal tract	83	-26	-20	29
Body of corpus callosum	34	-17	-16	35
Left Putamen	24	-16	10	-15
Right Inferior longitudinal fasciculus	21	48	-19	-20
Right Cingulum (cingulate gyrus)	20	9	11	30

4. DISCUSSION

The current results show that it is possible to classify control and TS children with a high degree of accuracy using an automated procedure that combines TBSS with SVM. Our results achieved a highest accuracy of 88.04% better than some previous work which using resting-state functional connectivity(RSFC) MRI [14] to compare functional connectivity of the basal ganglia with RSFC MRI-defined cortical systems, subsequently combining SVM and RSFC MRI for TS children classification [15], being able to classify group membership with 74% accuracy. It is worth noting that no significant AD change were found between the groups in our statistical results that are corrected for multiple comparisons, but the AD voxels feature sets selected by ReliefF achieved the most accurate classification using SVM. The reason for this lies in methodological differences between the two approaches. For TBSS, each voxel is assigned a t-value that is corrected for multiple comparisons, The level of correction for multiple comparisons is therefore extremely high due to the large number of total voxels (157,502 voxels) to be considered. However, the SVM approach is underpinned by a different theoretical framework. Following the most salient voxels are selected by the ReliefF algorithm, the majority of voxels in the WM skeleton are discarded as irrelevant for subsequent SVM classification. Therefore, the SVM only considers the voxels identified by ReliefF in its calculation of a single parameter per subject, and does not run into the problem of multiple comparison biases.

The current work also identifies the regions selected by the ReliefF that are most influential for classification. The largest 5 clusters of voxels were located in left corticospinal tract and putamen, body of corpus callosum, right Inferior longitudinal fasciculus and cingulum (cingulate gyrus). Tics are the hallmark of TS, so the involvement of the corticospinal tract fits in well with clinical symptoms. Inferior longitudinal fasciculus and cingulum are long association fiber bundles. The modulation of tics by cortical activation depends on the long association fibre bundles within one hemisphere [16]. Our results conform to the previous study with TBSS which showed AD increase in these WM tracts [5]. The corpus callosum is the biggest commissural fibers and transfers information between the hemispheres. The corpus callosum is supposed to play an important role in modulation of tics by mediating the inhibiting influence by prefrontal cortices. The increased AD values in the body of corpus callosum in our data could be responsible for a diminished inhibitory influence. The increased AD in the putamen is discussed as a result of disrupted white matter projections to the globus pallidus and the microstructure change of globus pallidus led to some useful information cannot be passed to the cerebral cortex, causing the tics[17]. It also tallies with our result.

It is worth emphasizing that our study used the nested CV for evaluating the accuracy and the feature selection method using ReliefF was corporated into the nested CV. While some other studies [6, 12, 18] employed feature selection on the full dataset which may be overly optimistic, the evaluation method in our study is a better estimation of generalization.

5. CONCLUSION

The present study demonstrates the efficacy of using TBSS in conjunction with SVM to classify healthy and TS children. A fully automated procedure of this method is an appealing alternative to TS classification by the DSM which is both subjective and time consuming. These results support the contention that our methods may be useful for the early identification of subjects with TS, and hold promise for predicting prognosis and treatment outcome for individuals with TS.

ACKNOWLEDGEMENTS

This work was supported by 863 Projects (2013AA013803), National Natural Science Foundation of China (61271151, 91520202, 31271161), Youth Innovation Promotion Association CAS and Beijing Municipal Administration of Hospitals Incubating Program (PX2016035).

REFERENCES

[1] Makki, M.I., Behen, M., Bhatt, A., Wilson, B., Chugani, H.T., "Microstructural abnormalities of striatum and thalamus in children with Tourette syndrome. Movement disorders," official journal of the Movement Disorder Society 23, 2349-2356 (2008)

[2] Ganos, C., Roessner, V., Munchau, A., "The functional anatomy of Gilles de la Tourette syndrome," Neurosci Biobehav R 37, 1050-1062 (2013)

[3] Association, A.P., "Diagnostic and statistical manual of mental disorders : DSM-IV-TR," Corsini Encyclopedia of Psychology (2000)

[4] Smith, S.M., Jenkinson, M., Johansen-Berg, H., Rueckert, D., Nichols, T.E., Mackay, C.E., Watkins, K.E., Ciccarelli, O., Cader, M.Z., Matthews, P.M., Behrens, T.E., "Tract-based spatial statistics: voxelwise analysis of multi-subject diffusion data," Neuroimage 31, 1487-1505 (2006)

[5] Liu, Y., Miao, W., Wang, J., Gao, P., Yin, G., Zhang, L., Lv, C., Ji, Z., Yu, T., Sabel, B.A., He, H., Peng, Y., "Structural abnormalities in early Tourette syndrome children: a combined voxel-based morphometry and tract-based spatial statistics study," Plos One 8, e76105 (2013)

[6] O'Dwyer, L., Lamberton, F., Matura, S., Scheibe, M., Miller, J., Rujescu, D., Prvulovic, D., Hampel, H., "White Matter Differences between Healthy Young ApoE4 Carriers and Non-Carriers Identified with Tractography and Support Vector Machines," Plos One 7, (2012)

[7] Calderoni, S., Retico, A., Biagi, L., Tancredi, R., Muratori, F., Tosetti, M., "Female children with autism spectrum disorder: an insight from mass-univariate and pattern classification analyses," Neuroimage 59, 1013-1022 (2012)

[8] Shiva, K., Ryan, N.S., Malone, I.B., Marc, M., David, C., Ridgway, G.R., Hui, Z., Fox, N.C., Sebastien, O., "The Importance of Group-Wise Registration in Tract Based Spatial Statistics Study of Neurodegeneration: A Simulation Study in Alzheimer's Disease," Plos One 7, e45996-e45996 (2012)

[9] Smith, S.M., Nichols, T.E., "Threshold-free cluster enhancement: addressing problems of smoothing, threshold dependence and localisation in cluster inference," Neuroimage 44, 83-98 (2009)

[10] Kononenko, I., "Estimating attributes: analysis and extensions of RELIEF," Proceedings of the European conference on machine learning on Machine Learning, pp. 171-182. Springer-Verlag New York, Inc., Catania, Italy (1994)

[11] Grana, M., Termenon, M., Savio, A., Gonzalez-Pinto, A., Echeveste, J., Perez, J.M., Besga, A., "Computer aided diagnosis system for Alzheimer disease using brain diffusion tensor imaging features selected by Pearson's correlation," Neuroscience letters 502, 225-229 (2011)

[12] O'Dwyer, L., Lamberton, F., Bokde, A.L.W., Ewers, M., Faluyi, Y.O., Tanner, C., Mazoyer, B., O'Neill, D., Bartley, M., Collins, D.R., Coughlan, T., Prvulovic, D., Hampel, H., "Using Support Vector Machines with Multiple Indices of Diffusion for Automated Classification of Mild Cognitive Impairment," Plos One 7, (2012)
[13] Wilson, S.M., Ogar, J.M., Laluz, V., Growdon, M., Jang, J., Glenn, S., Miller, B.L., Weiner, M.W., Gorno-Tempini, M.L., "Automated MRI-based classification of primary progressive aphasia variants," Neuroimage 47, 1558-1567 (2009)
[14] Greene, D.J., Laumann, T.O., Dubis, J.W., Ihnen, S.K., Neta, M., Power, J.D., Pruett, J.R., Black, K.J., Schlaggar, B.L., "Developmental Changes in the Organization of Functional Connections between the Basal Ganglia and Cerebral Cortex," J Neurosci 34, 5842-5854 (2014)
[15] Richards, C.A., Black, K.J., "Tourette Syndrome research highlights 2014," F1000Research 4, 69 (2015)
[16] Church, J.A., Fair, D.A., Dosenbach, N.U.F., Cohen, A.L., Miezin, F.M., Petersen, S.E., Schlaggar, B.L., "Control networks in paediatric Tourette syndrome show immature and anomalous patterns of functional connectivity," Brain 132, 225-238 (2009)
[17] Neuner, I., Kupriyanova, Y., Stocker, T., Huang, R.W., Posnansky, O., Schneider, F., Shah, N.J., "Microstructure assessment of grey matter nuclei in adult tourette patients by diffusion tensor imaging," Neuroscience letters 487, 22-26 (2011)
[18] Haller, S., Nguyen, D., Rodriguez, C., Emch, J., Gold, G., Bartsch, A., Lovblad, K.O., Giannakopoulos, P., "Individual prediction of cognitive decline in mild cognitive impairment using support vector machine-based analysis of diffusion tensor imaging data," Journal of Alzheimer's disease : JAD 22, 315-327 (2010)